

# Bayesian estimation with Gauss-Markov-Potts priors in optical diffraction tomography

Hacheme Ayasso, Bernard Duchêne and Ali Mohammad Djafari  
Laboratoire des Signaux et Systèmes (L2S, UMR 8506: CNRS - SUPELEC - Univ Paris Sud 11)  
Supélec, Plateau de Moulon, 91192 Gif-sur-Yvette, FRANCE.

## ABSTRACT

In this paper, Optical Diffraction Tomography (ODT) is considered as an inverse scattering problem. The goal is to retrieve a map of the electromagnetic parameters of an unknown object from measurements of the scattered electric field that results from its interaction with a known interrogating wave. This is done in a Bayesian estimation framework. A Gauss-Markov-Potts prior appropriately translates the a priori knowledge that the object is made of a finite number of homogeneous materials distributed in compact homogeneous regions. First, we express the *a posteriori* distributions of all the unknowns and then a Gibbs sampling algorithm is used to generate samples and estimate the posterior mean of the unknowns. Some preliminary results, obtained by applying the inversion algorithm to experimental laboratory controlled data, will illustrate the performances of the proposed method that is compared to the more classical Contrast Source Inversion method (CSI) developed in a deterministic framework.

**Keywords:** Optical diffraction tomography, Bayesian approach, Gauss-Markov-Potts prior, Monte Carlo Markov Chain sampling

## 1. INTRODUCTION

During the last few years, optical diffraction tomography has gained a lot of interest in several domains such as 3D imaging of biological samples which can reveal intracellular structures<sup>1</sup> or nondestructive testing of nanoscale objects<sup>2</sup> with characteristic dimensions of the order of the interrogating wavelength. Optical diffraction tomography is considered, herein, as an inverse scattering problem where the goal is to retrieve a map of a contrast function depending upon the electromagnetic parameters (the dielectric permittivity or the refraction index) of an unknown object from measurements of the scattered field that results from the interaction between this object and a known interrogating (or incident) wave. This technique allows us to retrieve an image of the whole object contrarily to other methods such as electronic or atomic force microscopy that only yield an image of the object surface. The recent development of this technique has been made possible thanks to the appearance of interferometry techniques able to provide accurate phase measurements. This has made possible the application of inversion methods already known in other domains such as microwave or ultrasonic imaging.

The major challenge in ODT is the ill-posed nature of the inverse problem, which requires a regularization that consists in introducing prior information in order to reduce the dimension of admissible solution space. Moreover, the exact formulation of the associated direct problem, which would consist in computing the scattered field knowing the object and the incident field, leads to a non-linear forward model, which renders the resolution of the inverse problem more involved. Different solution methods has been proposed in the literature; they can be classified according to the way they handle the non-linearity, or to the way used to introduce prior information. More details on the state of the art are given in <sup>3</sup>.

Herein, the available a priori information on the sought object is taken into account by means of a Bayesian approach with a Gauss-Markov-Potts prior and the non-linear forward model is inverted in a joint estimation framework. This approach has already been applied with success to microwave imaging. However, in the latter case multi-frequency scattered field data were available all around the object, whereas, in the present case, only

---

Further author information: (Send correspondence to Hacheme Ayasso)

Hacheme Ayasso: E-mail: ayasso@lss.supelec.fr, Telephone: +33 (0)1 69 85 17 43

Bernard Duchêne : E-mail: duchene@lss.supelec.fr, Telephone: +33 (0)1 69 85 15 57

Ali Mohammad-Djafari : E-mail: djafari@lss.supelec.fr, Telephone: +33 (0)1 69 85 17 41

single-frequency aspect-limited data are measured in a restricted domain for a few illumination directions, which makes the inversion task more difficult and the introduction of prior information more important.

The paper is organized as follows: section 2 displays the measurement configuration and the corresponding forward model. Section 3 details the Bayesian approach, with the prior models that account for the prior information available on the unknowns, and the stochastic sampling approximation technique (Gibbs sampler) used to overcome the intractable character of the estimator derived from the prior model. In section 4, the validity of the forward model and the performances of the inversion algorithm are checked by using experimental data (courtesy of Institut Fresnel). Finally, a conclusion and some perspectives are given in section 5.

## 2. FORWARD MODEL

This section describes the measurement configuration used to collect the data and the forward model that links the scattered field to the object under test.

### 2.1 Configuration

Let us consider an object, with cross section  $\Omega$ , located in the upper layer of a stratified medium (see figure 1) made of two semi-infinite half-spaces,  $\mathcal{D}_1$  and  $\mathcal{D}_2$ , separated by a planar interface  $\gamma_{12}$ . We denote as  $\epsilon_1$  and  $\epsilon_2$  the relative dielectric permittivity of the two half-spaces, respectively, and we assume that the different media are lossless. The object is supposed to be contained in a test domain  $\mathcal{D}$  completely contained in the upper half-space ( $\Omega \subset \mathcal{D} \subset \mathcal{D}_1$ ) and is characterized by a contrast function  $\chi(\mathbf{r})$  defined in  $\mathcal{D}$  and null outside  $\Omega$ .

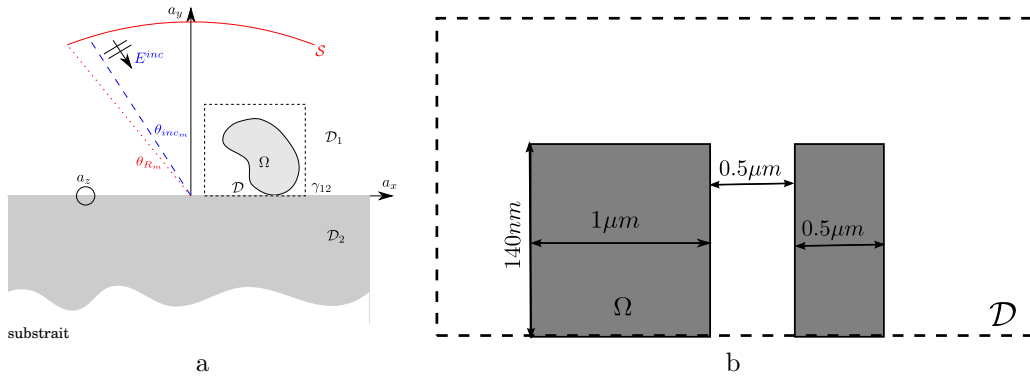


Figure 1. a) Measurement configuration, b) object under test

The object is considered as infinite and invariant along the  $Oz$  axis perpendicular to the plane of Figure 1 and is illuminated by a plane wave whose electric field is polarized along the  $Oz$  direction and whose implied time-dependence is chosen as  $\exp(-i\omega t)$ . By assuming that the different media are not depolarizing, this leads to a two-dimensional transverse magnetic polarization case with a scalar electric field formulation. The direction of illumination  $\theta_{inc}$  can be varied in the angular sector  $\pm\theta_{inc,m}$  and  $N_{inc}$  views are realized at varying  $\theta_{inc}$ , each view being constituted of measurements of the scattered field at  $N_{rec}$  receiver positions located in the measurement domain  $\mathcal{S}$  ( $\mathcal{S} \subset \mathcal{D}_1$ ) in the far field, in directions  $\theta_{rec}$  such that  $|\theta_{rec}| \leq \theta_{rec,m}$ .

### 2.2 Formulation

Let us define the object contrast function  $\chi$  as:

$$\chi(\mathbf{r}) = k_m^2(\mathbf{r}) - k_1^2, \quad \forall \mathbf{r} \in \mathcal{D}, \quad (1)$$

where  $k_m$  is the propagation constant of medium  $m$  such that  $k_m^2 = \omega^2 \epsilon_0 \epsilon_m \mu_0$  ( $m = 1, 2, \Omega$ ),  $\epsilon_0$  and  $\mu_0$  are the dielectric permittivity and the magnetic permeability of free space ( $\epsilon_0 = 8.854 \times 10^{-12} \text{F/m}$ ,  $\mu_0 = 4\pi \times 10^{-7} \text{H/m}$ ),

respectively,  $\omega$  is the angular frequency and  $\epsilon_m$  is the relative dielectric permittivity of medium  $m$ . The forward problem consists then in finding the scattered field  $E^{scat}(\mathbf{r}')$ ,  $\mathbf{r}' \in \mathcal{S}$ , knowing the contrast function  $\chi(\mathbf{r})$ ,  $\mathbf{r} \in \mathcal{D}$ , whereas the inverse problem consists in finding  $\chi(\mathbf{r})$ , given measurements of the scattered field  $E^{scat}$ .

The forward model is described through domain integral representations of the electric field. Hence, by applying Green's theorem to the Helmholtz wave equation satisfied by the fields and by accounting for continuity and radiation conditions, we get two coupled electric field integral equations. The first one is denoted as observation equation as it links the observations (the scattered field) to the contrast function:

$$E^{scat}(\mathbf{r}) = \int_{\mathbf{r}' \in \mathcal{D}} \mathcal{G}^o(\mathbf{r}, \mathbf{r}') E^{tot}(\mathbf{r}') \chi(\mathbf{r}') d\mathbf{r}', \quad \forall \mathbf{r} \in \mathcal{S}. \quad (2)$$

$\mathcal{G}$  is the Green's function that accounts for the measurement configuration and represents the radiation of a line source located in  $\mathbf{r}'$  and observed in  $\mathbf{r}$  in the absence of the object; superscript  $o$  stands for "observation" and means that source and observation are located in  $\mathcal{D}$  and  $\mathcal{S}$ , respectively.  $E^{tot}$  is the unknown total electric field. The above equation can be rewritten in terms of the Huyghens-type sources  $w$  induced within the target by the incident wave (the induced currents), i.e.  $w(\mathbf{r}') = \chi(\mathbf{r}') E^{tot}(\mathbf{r}')$ :

$$E^{scat}(\mathbf{r}) = \int_{\mathbf{r}' \in \mathcal{D}} \mathcal{G}^o(\mathbf{r}, \mathbf{r}') w(\mathbf{r}') d\mathbf{r}', \quad \forall \mathbf{r} \in \mathcal{S}. \quad (3)$$

The second equation is denoted as coupling (or state) equation and it links the unknown total field  $E^{tot}$  in  $\mathcal{D}$  to the induced sources:

$$E^{tot}(\mathbf{r}) = E^o + \int_{\mathbf{r}' \in \mathcal{D}} \mathcal{G}^c(\mathbf{r}, \mathbf{r}') w(\mathbf{r}') d\mathbf{r}', \quad \forall \mathbf{r} \in \mathcal{D}, \quad (4)$$

where superscript  $c$  stands for "coupling" and indicates that the Green's function has both source and observation points located in  $\mathcal{D}$ .  $E^o$  is the total field that would exist in  $\mathcal{D}$  in the absence of object, i.e.:

$$E^o = e^{-ik_1(x \cos(\theta_{inc}) + y \sin(\theta_{inc}))} - R(k_1 \sin(\theta_{inc})) e^{ik_1(x \cos(\theta_{inc}) + y \sin(\theta_{inc}))}, \quad (5)$$

with

$$R(\alpha) = \frac{\beta_1(\alpha) - \beta_2(\alpha)}{\beta_1(\alpha) + \beta_2(\alpha)} \quad (6)$$

$$\beta_m(\alpha) = \sqrt{k_m^2 - \alpha^2}, \quad \Im m(\beta_m) \geq 0, \quad m = 1, 2. \quad (7)$$

In order to complete the forward model, the expressions of Green's functions ( $\mathcal{G}^o$  and  $\mathcal{G}^c$ ) are now given. First let us recall that a stratified medium is considered and that, for both functions, the source point  $\mathbf{r}' = (x', y')$  and the observation point  $\mathbf{r} = (x, y)$  are located in medium  $\mathcal{D}_1$ . This leads to the general expression:

$$\mathcal{G}(\mathbf{r}, \mathbf{r}') = \int_{-\infty}^{+\infty} \frac{i}{4\pi\beta_1} \left[ \exp(i\beta_1(\alpha)|x - x'|) + R(\alpha) \exp(i\beta_1(\alpha)(x + x')) \right] \exp(i\alpha(y - y')) d\alpha. \quad (8)$$

which is that of the coupling Green's function ( $\mathcal{G}^c(\mathbf{r}, \mathbf{r}') = \mathcal{G}(\mathbf{r}, \mathbf{r}')$ ). For the observation Green's function, an approximation can be made since the scattered field is observed in the far field. Hence, by noting that observation  $\mathbf{r} = (r, \theta)$  is made at constant  $r$  in directions  $\theta$  such that  $x > x'$  and by getting rid of the  $r$  dependence, it can be written as:

$$\mathcal{G}^o(\mathbf{r}, \mathbf{r}') = \frac{\zeta(\theta, \mathbf{r}')}{2\pi} \int_{-\infty}^{+\infty} \frac{i}{2\beta_1(\alpha)} \exp(i(\beta_1(\alpha)x + \alpha y)) d\alpha, \quad (9)$$

with  $\zeta(\theta, \mathbf{r}') = [\exp(-i\beta_1(\alpha_\theta)x') + R(\alpha_\theta) \exp(i\beta_1(\alpha_\theta)x')] \exp(-i\alpha_\theta y)$  and  $\alpha_\theta = k_1 \sin(\theta)$ .

Discrete versions of observation and coupling equations are obtained by applying the method of moments with pulse basis functions and point matching. This results in partitioning the test domain into  $N_{\mathcal{D}}$  elementary

square pixels small enough to consider the fields and the contrast as constant over each of them. This leads to the following linear systems where the unknowns are the values of sources and fields at the centres of the pixels:

$$\mathbf{E}^{scat} = \mathbf{G}^o \mathbf{w} \quad (10)$$

$$\mathbf{E}^{tot} = \mathbf{E}^o + \mathbf{G}^c \mathbf{w}, \quad (11)$$

where  $\mathbf{G}^o$  and  $\mathbf{G}^c$  are two matrices whose elements are calculated by integrating  $\mathcal{G}^o$  and  $\mathcal{G}^c$ , respectively, over the elementary square pixels. In practice  $\mathbf{G}^c$  and  $\mathbf{G}^o$  are obtained in the spectral and spatial domains, respectively. Details on such computations in stratified media can be found in <sup>4</sup>.

### 3. BAYESIAN APPROACH

As any inverse scattering problem, optical diffraction tomography suffers from ill-posedness and non-linearity. Hence, ill-posedness is overcome by introducing prior information in the inversion algorithm, while non-linearity is dealt with through a joint estimation of induced currents  $w$  and contrast  $\chi$ , which turns the problem into a bilinear one. Herein, a Bayesian inference framework allows us to introduce prior information using a probabilistic approach. The forward model is rewritten in terms of the induced sources and additional noise terms,  $\epsilon$  and  $\xi$  (denoted as observation and coupling errors, respectively), are added in order to account for the different errors: measurement uncertainties and model errors (discretization and other approximations):

$$\mathbf{E}^{scat} = \mathbf{G}^o \mathbf{w} + \epsilon \quad (12)$$

$$\mathbf{w} = \chi \mathbf{E}^o + \chi \mathbf{G}^c \mathbf{w} + \xi \quad (13)$$

In a Bayesian framework, the posterior law of all the unknowns given the data  $p(\mathbf{w}, \chi | \mathbf{E}^{scat})$  is expressed, according to Bayes formula, as:

$$p(\mathbf{w}, \chi | \mathbf{E}^{scat}) = \frac{p(\mathbf{E}^{scat} | \mathbf{w}, \chi) p(\mathbf{w}, \chi)}{p(\mathbf{E}^{scat})}, \quad (14)$$

where  $p(\mathbf{E}^{scat} | \mathbf{w}, \chi)$  is the likelihood,  $p(\mathbf{w}, \chi)$  is the prior model and  $p(\mathbf{E}^{scat})$  is the evidence of the model. The likelihood can be obtained from the forward and noise ( $\epsilon$ ) models, while the prior model is usually dedicated to the application. Once the posterior law has been obtained, optimal values of unknowns are computed using an appropriate estimator. In the literature, two widely used estimators do appear: the Maximum A Posteriori (MAP) such that  $\text{MAP}\{\hat{w}, \hat{\chi}\} = \arg \max_{(\mathbf{w}, \chi)} (p(\mathbf{w}, \chi | \mathbf{E}^{scat}))$  and the Posterior Mean (PM) such that:

$$\hat{\mathbf{a}} = \int \int \mathbf{a} \cdot p(\mathbf{w}, \chi | \mathbf{E}^{scat}) d\mathbf{w} d\chi, \quad \mathbf{a} = \mathbf{w}, \chi. \quad (15)$$

Herein, however, a closed-form expression of the estimator is not available and an approximation should be made in order to obtain a tractable solution. Hence, a Monte-Carlo Markov Chain (MCMC) sampler, associated with a PM empirical estimator, is used to approximate the posterior law numerically.

In the following, the model error distribution is defined in order to express the likelihood. Then, a Gauss-Markov-Potts prior model, which accounts for available prior information, is detailed. Finally, the estimator is discussed and the general layout of the inversion algorithm is given.

#### 3.1 Error modeling

The observation error is chosen in a classical way:  $\epsilon$  is supposed to be centered, white and with a fixed variance  $\rho_\epsilon^2$ . This leads to a Gaussian law  $p_\epsilon(\epsilon) = \mathcal{N}(\mathbf{0}, \rho_\epsilon^2 \mathbf{I})$ . Then, using the observation equation, the likelihood reads:

$$p(\mathbf{E}^{scat} | \mathbf{w}) = p_\epsilon(\mathbf{E}^{scat} - \mathbf{G}^o \mathbf{w}) = \left( \frac{1}{2\pi\rho_\epsilon^2} \right)^{\frac{N_{rec} + N_{inc}}{2}} \exp \left( - \frac{\|\mathbf{E}^{scat} - \mathbf{G}^o \mathbf{w}\|_{\mathcal{S}}^2}{2\rho_\epsilon^2} \right), \quad (16)$$

where  $\rho_\epsilon$  is supposed to be unknown and  $\|\cdot\|_{\mathcal{S}}$  is the norm associated to the inner product in  $L^2(\mathcal{S})$ . In the same way, the coupling error  $\xi$  is considered to be Gaussian with zero mean and unknown variance  $\rho_\xi^2$ , i.e.  $p_\xi(\xi) = \mathcal{N}(\mathbf{0}, \rho_\xi^2 \mathbf{I})$ .

### 3.2 Hierarchical prior model

The most important point in the present approach is the choice the prior distributions that account for the available information about the unknowns. For the current density  $\mathbf{w}$ , the only prior information that will be used is provided by the coupling equation. By assuming that  $\xi$  is a Gaussian distribution, the prior  $p(\mathbf{w}|\chi)$  reads:

$$p(\mathbf{w}|\chi) \propto \exp\left(\frac{-1}{2\rho_\xi^2}\|\mathbf{w} - \chi\mathbf{E}^o - \chi\mathbf{G}^c\mathbf{w}\|_{\mathcal{D}}^2\right). \quad (17)$$

As for the contrast  $\chi$ , the objects considered herein are man-made and known to be composed of a finite number  $N_\kappa$  of homogeneous materials distributed in compact regions. This prior information is introduced via a variable  $z(\mathbf{r})$ ,  $z(\mathbf{r}) \in \{1, \dots, N_\kappa\}$ , which represents the material (class) of pixel  $\mathbf{r}$ . The set of labels  $z(\mathbf{r}), \forall \mathbf{r} \in \mathcal{D}$ , is a hidden field. It represents the segmentation image for the contrast variable. Homogeneity inside a given region  $z$  is expressed by means of a Gaussian distribution:

$$p(\chi(\mathbf{r})|z(\mathbf{r}) = \kappa) = \mathcal{N}(m_\kappa, \rho_\kappa^2). \quad (18)$$

Hence, all the pixels with label  $\kappa$  belong to the same material whose properties are described by a law with mean value  $m_\kappa$  and variance  $\rho_\kappa^2$ . Furthermore, concerning the spatial dependence between the different pixels,

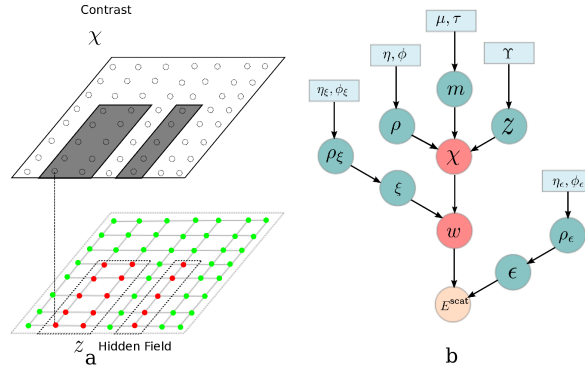


Figure 2. a) Prior model of contrast with hidden field b) hierarchical prior model

the pixels, given their classes, are supposed to be independent *a priori*. Hence, by accounting for the fact that  $\chi$  is positive, we get:

$$p(\chi|z) \propto \exp\left(-\frac{1}{2}(\chi - \mathbf{m}_z)^T \Sigma_z^{-1}(\chi - \mathbf{m}_z)\right) \mathbb{1}_{\chi \geq 0}, \quad (19)$$

where  $\mathbf{m}_z = \{m_{z(r_i)}, i = 1, \dots, N_{\mathcal{D}}\}$ ,  $\Sigma_z = \text{diag}(\rho_{z(r_i)}^2, i = 1, 2, \dots, N_{\mathcal{D}})$  and  $\mathbb{1}_{\chi \geq 0}$  represents the positivity constraint on  $\chi$ . Another Gauss-Markov prior, not considered herein, could be used to enhance the homogeneity inside a class.

As for the compactness of the regions, it is accounted for by means of a Markovian prior, which expresses the dependence between the label  $z(\mathbf{r})$  of the pixel  $\mathbf{r}$  and those ( $z(\mathbf{r}')$ ) of its neighbors  $\mathbf{r}'$  ( $\mathbf{r}' \in \mathcal{V}(\mathbf{r})$ , where  $\mathcal{V}(\mathbf{r})$  is a neighborhood of  $\mathbf{r}$  herein made of the nearest four pixels). This is translated by means of a Potts model:

$$p(z) = \frac{1}{\Xi} \exp\left(\frac{\Upsilon}{2} \sum_{\mathbf{r} \in \mathcal{D}} \sum_{\mathbf{r}' \in \mathcal{V}_{\mathbf{r}}} \delta(z(\mathbf{r}) - z(\mathbf{r}'))\right), \quad (20)$$

where  $\Xi$  is a normalization factor and  $\Upsilon$  a constant which determines the degree of correlation between neighbors.

The shaping parameters used in the previous priors are denoted as the hyper-parameters of the model and gathered in a variable  $\psi$  ( $\psi = \{\mathbf{m}_z, \Sigma_z, \rho_c^2, \rho_\xi^2\}$ ). Their values are unknown and need to be estimated, which

is done, simultaneously with the other unknowns of the problem, by choosing conjugate priors. Hence, Inverse Gamma and Gaussian distributions are assigned to the variances and to the means, respectively:

$$p(\rho_\epsilon^2) = \mathcal{IG}(\eta_\epsilon, \phi_\epsilon), \quad p(\rho_\xi^2) = \mathcal{IG}(\eta_\xi, \phi_\xi) \quad (21)$$

$$p(\rho_\kappa^2) = \mathcal{IG}(\eta, \phi), \quad p(m_\kappa) = \mathcal{N}(\mu, \tau), \quad \kappa = 1, \dots, N_\kappa,$$

where  $\{\eta, \phi, \eta_\epsilon, \phi_\epsilon, \eta_\xi, \phi_\xi, \mu, \tau\}$ , denoted as the *meta-hyper-parameters*, are fixed for a given problem and are chosen to have non-informative priors.

### 3.3 MCMC sampling

Now, we have all the ingredients to define the estimator. First, the joint posterior distribution for all the unknowns is expressed:

$$p(\mathbf{w}, \boldsymbol{\chi}, \mathbf{z}, \boldsymbol{\psi} | \mathbf{E}^{scat}) = \frac{p(\mathbf{E}^{scat} | \mathbf{w}, \rho_\epsilon^2) p(\mathbf{w} | \boldsymbol{\chi}, \rho_\xi^2) p(\boldsymbol{\chi} | \mathbf{z}, \mathbf{m}_z, \Sigma_z) p(\mathbf{z}) p(\boldsymbol{\psi})}{p(\mathbf{E}^{scat})}. \quad (22)$$

In order to obtain the values of all unknowns, an estimator (MAP or PM) should be used. However, both of the above-mentioned estimators are intractable. Hence, the posterior law should be approximated. This is done by using a MCMC sampling method. The idea is to draw samples according to the posterior law. Once a sufficient number of samples  $N_{sam}$  has been obtained, the unknowns can be calculated using an empiric estimator. We define the empiric PM estimator as:

$$\hat{\boldsymbol{\chi}} = \frac{1}{N_{sam}} \sum_{i=1}^{N_{sam}} \boldsymbol{\chi}^i, \quad (23)$$

where  $\boldsymbol{\chi}^i$  are the samples of the joint posterior distribution. A Gibbs sampler is used herein; it draws samples according to marginal posterior laws. The general flow chart of the algorithm is as follows. First, an initialization step yields initial values of the different variables<sup>3</sup>: hence,  $\mathbf{w}^0$  is obtained by back-propagating the scattered field data from  $\mathcal{S}$  onto  $\mathcal{D}$ , then  $\boldsymbol{\chi}^0$  is obtained from the coupling equation and the source constitutive relationship and a *K-means algorithm*<sup>5</sup> is used to get  $\mathbf{z}^0$ ; finally, from  $\mathbf{w}^0$ ,  $\boldsymbol{\chi}^0$  and  $\mathbf{z}^0$ , an empiric estimator provides  $\boldsymbol{\psi}^0$ . Then, the sources, the contrast, the hidden field and the hyper-parameters are looked for iteratively. Iteration step  $n$  reads:

1. sample  $\mathbf{w}^n$  from  $p(\mathbf{w} | \mathbf{E}^{scat}, \boldsymbol{\chi}^{n-1}, \mathbf{z}^{n-1}, \boldsymbol{\psi}^{n-1})$ ,
2. sample  $\boldsymbol{\chi}^n$  from  $p(\boldsymbol{\chi} | \mathbf{w}^n, \boldsymbol{\psi}^{n-1}, \mathbf{z}^{n-1})$ ,
3. sample  $\mathbf{z}^n$  from  $p(\mathbf{z} | \boldsymbol{\chi}^n, \boldsymbol{\psi}^{n-1})$ ,
4. sample  $\boldsymbol{\psi}^n$  from  $p(\boldsymbol{\psi} | \mathbf{w}^n, \boldsymbol{\chi}^n, \mathbf{E}^{scat}, \mathbf{z}^n)$ .

Steps 1 to 4 are iterated until convergence. It is proven<sup>6</sup> that the samples converge toward samples from the joint law after a number  $N_{min}$  of warm-up steps. Thanks to the choice of conjugate priors, the sampling according to the marginal posteriors can be done relatively easily. For  $\mathbf{w}$ , the marginal posterior gives a multivariate Gaussian distribution:

$$p(\mathbf{w} | \mathbf{E}^{scat}, \boldsymbol{\chi}, \mathbf{z}, \boldsymbol{\psi}) \propto \exp\left(-\frac{J(\mathbf{w})}{2\rho_\epsilon^2}\right), \quad (24)$$

with

$$J(\mathbf{w}) = \|\mathbf{E}^{scat} - \mathbf{G}^o \mathbf{w}\|_{\mathcal{S}}^2 + \frac{\rho_\epsilon^2}{\rho_\xi^2} \|\mathbf{w} - \boldsymbol{\chi} \mathbf{E}^o - \boldsymbol{\chi} \mathbf{G}^c \mathbf{w}\|_{\mathcal{D}}^2. \quad (25)$$

An optimization method can be used to sample it<sup>7</sup>. The contrast  $\boldsymbol{\chi}$  follows also a multivariate truncated Gaussian distribution:

$$p(\boldsymbol{\chi} | \mathbf{w}, \boldsymbol{\psi}, \mathbf{z}) \propto \exp\left(-\frac{\|\mathbf{w} - \boldsymbol{\chi} \mathbf{E}^{tot}\|_{\mathcal{D}}^2}{2\rho_\xi^2} - \frac{(\boldsymbol{\chi} - \mathbf{m}_z)^T \Sigma_z (\boldsymbol{\chi} - \mathbf{m}_z)}{2}\right) \mathbb{1}_{\boldsymbol{\chi} \geq 0}. \quad (26)$$

Sampling this distribution is easier since its components are independent. For the hidden field  $\mathbf{z}$ , we get a Potts field. Drawing samples according to this distribution is done by using another Gibbs sampler<sup>3</sup>. Finally, concerning the hyper-parameters  $\boldsymbol{\psi}$ , we find the same distributions for the posteriors of than for their priors, but with different shaping parameters:

$$\begin{aligned} p(\rho_\xi^2 | \mathbf{w}, \boldsymbol{\chi}) &= \mathcal{IG}(\tilde{\eta}_\xi, \tilde{\phi}_\xi), & p(\rho_\epsilon^2 | \mathbf{w}, \mathbf{E}^{scat}) &= \mathcal{IG}(\tilde{\eta}_\epsilon, \tilde{\phi}_\epsilon) \\ p(\rho_\kappa^2 | \boldsymbol{\chi}, \mathbf{z}) &= \mathcal{IG}(\tilde{\eta}_\kappa, \tilde{\phi}_\kappa), & p(m_\kappa | \boldsymbol{\chi}, \mathbf{z}) &= \mathcal{N}(\tilde{\mu}_\kappa, \tilde{\tau}_\kappa), \quad \kappa = 1, \dots, N_\kappa, \end{aligned} \quad (27)$$

where the tilded values are given<sup>3</sup>.

## 4. RESULTS

This section is devoted to the validation of the forward model and to the evaluation of the inversion algorithm against experimental data (courtesy of G. Maire, A. Sentenac and K. Belkebir). The latter come from a laboratory controlled experiment led at Institut Fresnel (Marseille, France) and thoroughly detailed in<sup>8</sup>. A laser, operating at a 633 nm wavelength, illuminates the object under  $N_{inc} = 8$  incident directions in the range  $\pm\theta_{inc_m} = 32^\circ$ , while the scattered field is observed in  $N_{rec} = 611$  receiving directions in the range  $\pm\theta_{rec_m} = 46^\circ$ , by means of a reflection microscope equipped with an interferometric device able to provide accurate measurements of the phase. The object under test is made of resin rods, whose relative permittivity is  $\epsilon_r = 2.66$  (see fig.1.b), deposited on a silicon substratum ( $\epsilon_2 = 15.07$ ), whereas the upper layer is air ( $\epsilon_1 = 1$ ). We partition the test domain  $\mathcal{D}$  into  $N_{\mathcal{D}} = 512 \times 32$  square pixels with a 7.4 nm side.

### 4.1 Model validation

In this section the object is supposed to be known and the model output is compared with the measured scattered field when the object is illuminated from direction  $\theta_{inc} = -15.22^\circ$ . It can be noted that the data are very noisy (and even missing) in directions close to the specular reflection. This is due to the fact that the scattered field is negligible as compared to the incident field in these directions and, hence, is hard to be accurately determined (for this reason, in practice only 586 scattered field data are available for each view). Despite this fact, computed and measured fields show an acceptable agreement far from the specular reflection (figure 3).

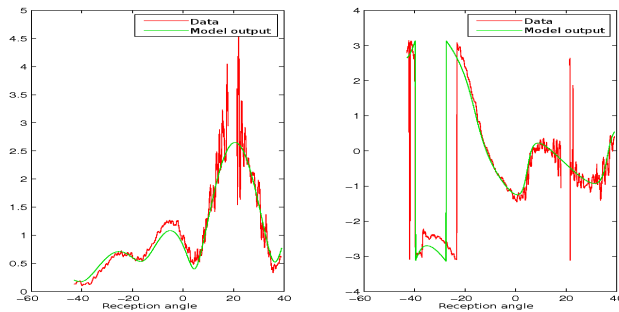


Figure 3. Amplitude (left) and phase (right) of the measured (red) and computed (green) scattered fields for an illumination direction of  $\theta_{inc} = -15.22^\circ$

### 4.2 Inversion results

Figure 4 displays the inversion results obtained with the above algorithm (denoted as MCMC): fig. 4-a displays a map of the contrast obtained after 512 iteration steps; it appears that the latter is retrieved in a satisfactory way concerning its value as well as its geometry. It is compared to the contrast obtained with the Contrast Source Inversion (CSI) method (fig. 4-b), a method developed in a deterministic framework which consists in looking alternately for the contrast and for the sources by minimizing a cost functional with a gradient-based method<sup>9</sup> and it appears that MCMC performs much better than the latter. This is confirmed by fig. 4-c which displays

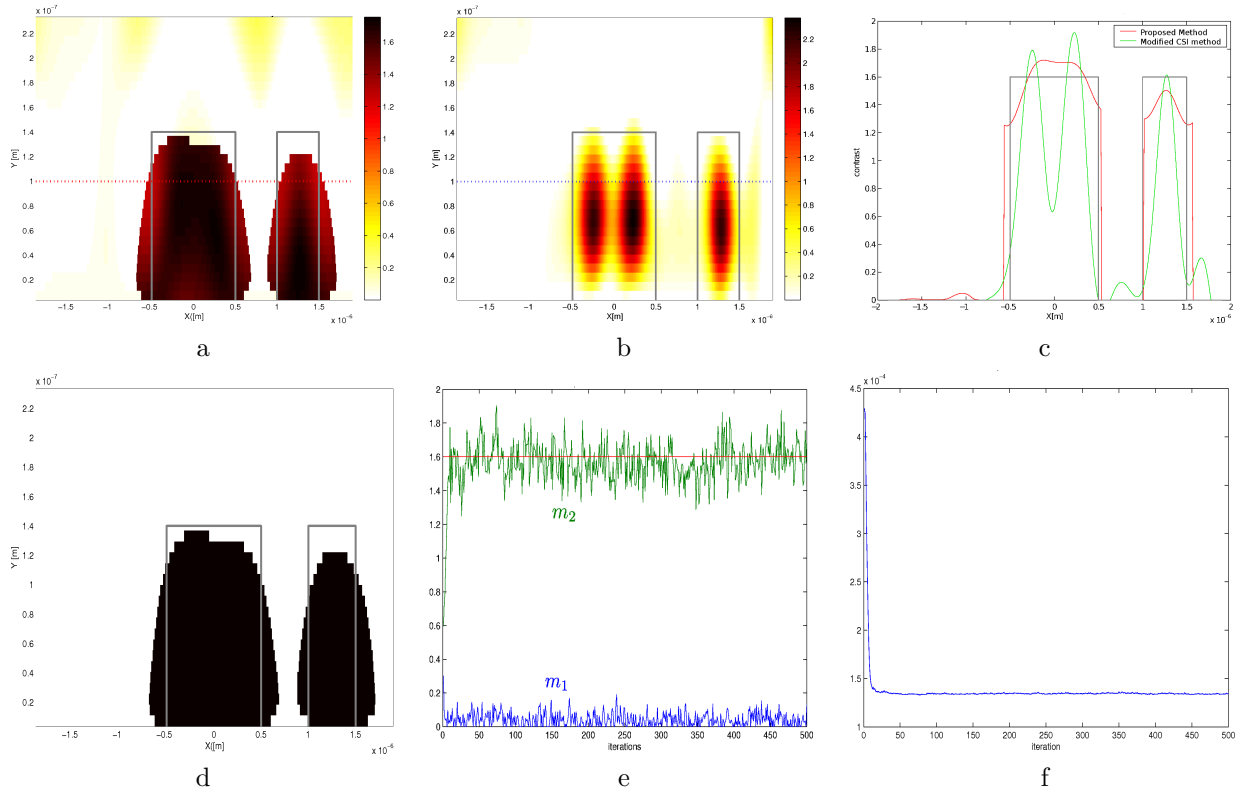


Figure 4. Reconstruction results: the contrast  $\chi$  obtained with MCMC (a) and CSI (b) and its profile at a height of 100 nm (c), the segmentation (hidden field  $z$ ) (d), the class means  $m_\kappa$  for classes  $\kappa = 1$  (air) and  $\kappa = 2$  (resin) (e) and the observation variance  $\rho_\epsilon^2$  (f)

the profiles obtained along a line at a height of 100 nm. From a computational time point of view, MCMC is less efficient than CSI as it takes twice more time than the latter, i.e. one hour for the above example on a PC with dual-core processor at a 2.66 GHz clock frequency, against 30 mn for CSI. Figures 4-d, -e and -f displays the segmentation results ( $z$ ) and the evolution of some of the hyper-parameters (the means of classes  $\kappa = 1$  (air) and  $\kappa = 2$  (resin) and the observation variance) during the iterative process.

## 5. CONCLUSION

In this paper optical diffraction tomography is considered as an inverse scattering problem and tackled in a Bayesian estimation framework, while a Gauss-Markov-Potts prior model accounts for the piece-wise homogeneity of the object. The joint estimation of object contrast, induced currents and other parameters of the model leads to intractable estimator. Hence, a Monte-Carlo Markov chain sampling method is used to approximate the posterior law and to calculate the PM estimator. This approach is checked using experimental data and satisfactory results are obtained.

The major drawback of above method is the required computational burden, essentially due to the MCMC stochastic sampling method. At the present time, another approximation method developed for Bayesian inference problems<sup>10</sup>, the so-called *variational Bayesian approach*, is under study. It allows a much faster approximation of the posterior laws than MCMC, as it is based upon an analytic approximation of the distribution, while it keeps small the approximation error. This time saving should be greatly appreciated in intricate configurations such as the one considered herein which concerns objects in stratified media and requires heavy computations.



## REFERENCES

- [1] Charrère, F., Kühn, J., Colomb, T., Cuhe, E., Marquet, P., and Depeursinge, C., “Sub-cellular quantitative optical diffraction tomography with digital holographic microscopy,” in [*Society of Photo-Optical Instrumentation Engineers (SPIE) Conference Series*], **6441**, 16 (2007).
- [2] Lauer, V., “New approach to optical diffraction tomography yielding a vector equation of diffraction tomography and a novel tomographic microscope,” *Journal of Microscopy* **205**(2), 165–176 (2002).
- [3] Ayasso, H., Duchêne, B., and Mohammad-Djafari, A., “Bayesian inversion for optical diffraction tomography,” *Journal of Modern Optics* **57**(9), 765–776 (2010).
- [4] Lesselier, D. and Duchêne, B., “Buried, 2-D penetrable objects illuminated by line-sources: FFT-based iterative computations of the anomalous field,” in [*Application of Conjugate Gradient Methods to Electromagnetics and Signal Analysis*], *PIER*(5), 400–438, T. K. Sarkar, Elsevier, New York (1991).
- [5] MacQueen, J., “Some methods for classification and analysis of multivariate observations,” in [*5th Berkeley Symposium on Mathematical Statistics and Probability*], **1**, 281–297, Western Management Sciences Institute UCLA, Los Angeles (1967).
- [6] Robert, C. and Casella, G., [*Monte Carlo Statistical Methods*], Springer Verlag, New York (2004).
- [7] Féron, O., Duchêne, B., and Mohammad-Djafari, A., “Microwave imaging of inhomogeneous objects made of a finite number of dielectric and conductive materials from experimental data,” *Inverse Problems* **21**(6), 95 (2005).
- [8] Maire, G., Drsek, F., Girard, J., Giovannini, H., Talneau, A., Konan, D., Belkebir, K., Chaumet, P. C., and Sentenac, A., “Experimental demonstration of quantitative imaging beyond Abbe’s limit with optical diffraction tomography,” *Physical Review Letters* **102**, 213905 (May 2009). PMID: 19519110.
- [9] van den Berg, P. M. and Kleinman, R. E., “A contrast source inversion method,” *Inverse Problems* **13**, 1607–1620 (1997).
- [10] Ayasso, H., Duchêne, B., and Mohammad-Djafari, A., “A variational Bayesian approach of inversion in optical diffraction tomography,” in [*Proceeding of the 11th Workshop on Optimization and Inverse Problems in Electromagnetism*], Sofia (September 2010).